Heat stress: an underestimated impact of climate change on vegetation

Nicolas Viovy
nicolas.viovy@lsce.ipsl.fr

Laboratoire des Sciences du Climat et de L'Environnement https://orcid.org/0000-0002-9197-6417
Philippe Ciais
Laboratoire des Sciences du Climat et de l'Environnement https://orcid.org/0000-0001-8560-4943
Ana Bastos
University of Leipzig
Fabienne Maignan
LSCE, IPSL https://orcid.org/0000-0001-5024-5928
Cedric Bacour
Laboratoire des Sciences du Climat et de L'Environnement
Marc Peaucelle
INRAE, Université de Bordeaux https://orcid.org/0000-0003-0324-4628

Biological Sciences - Article

Keywords:

Posted Date: September 20th, 2024

DOI: https://doi.org/10.21203/rs.3.rs-4964815/v1

Additional Declarations: There is **NO** Competing Interest.

heat stress: an underestimated impact of climate change on vegetation

Nicolas Viovy[1*], Philippe Ciais[1], Ana Bastos[2,3], Fabienne Maignan[1], Cédric Bacour[1] and Marc Peaucelle[4]

[1*]LSCE/IPSL, CEA/CNRS/Université Paris-Saclay, Bat 714 Orme des Merisiers, Gif-sur-Yvette, 91191, France.
[2]Department Biogeochemical Integration, Max Planck Institute for Biogeochemistry, Hans-Knöll-Str. 10 , Jena, D-07745, Germany.
[3]Institute for Earth System Science and Remote Sensing, Leipzig University, Talstr. 35, 04103 , Leipzig, D-07745, Germany.
[4]ISPA, INRAE, Bordeaux center, Villenave d'Ornon, 33882, France.

*Corresponding author(s). E-mail(s): nicolas.viovy@lsce.ipsl.fr;
Contributing authors: philippe.ciais@lsce.ipsl.fr;
ana.bastos@uni-leipzig.de; fabienne.maignan@lsce.ipsl.fr;
cedric.bacour@lsce.ipsl.fr; marc.peaucelle@inrae.fr;

Abstract

Heat stress occurs when plants experience temperature beyond their normal optimum and can disrupt cell functioning and growth. Exposure to extreme heat results in reduced plant productivity and have lagged effects through accelerated leaf senescence [1] [2]. Few studies exist on evaluation of impact of heat stress at the global scale. It not fully understand and is thereby only partially represented in land surface models. Detecting the impact of heat stress from space-borne observations is challenging, since it co-occurs with other stressors, such as low soil water availability and atmospheric dryness. We established a method that allows to detect the long term impact of heat stress at the global scale from optical remote sensing data by disentangling the direct heat stress effect from other covariates, particularly drought. Here we show that, when maximum surface temperature exceeds a threshold of around 43 °C, heat stress is detected on satellite estimates of Leaf Area Index (LAI).Locally, we observe a different critical temperature at which leaf damage occurs suggesting an acclimation of plants to heat stress. By implementing this empirical relationship in a land surface model to account for the lag effect on leaf. we simulate a limited impact of leaf heat damages on net primary productivity (NPP) until the beginning of the 21st century but a rapid increase in the last two decades (2000-2020). Simulations for future climate suggest that, if the direct heat induced reduction of NPP at the global scaleremain below 2% for a high warming scenario, it can reach 25% for China and western US. This study emphasizes more attention should be paid to the direct impact of heat stress on leaves in addition to the drought for predicting future vegetation carbon uptake.

1 Main

Recurrence of heatwaves has increased in the last decades [3], [4] with aglobal reocerd temperture in 2023 and several localrecord temperature in most of the regions of the earth in the last four years high temperature records ([5], [6]). These heatwaves are generally associated with droughts and have a strong negative impact on ecosystem productivity [7], [8], [9]. Several processes are known to impact ecosystem productivity during droughts and heatwaves. In the short term, stomatal closure, associated with increased atmospheric vapor pressure and soil water deficits, reduces CO_2 diffusion into the stomata, thereby limiting photosynthesis [10]. Another effect is the direct inhibition of photosynthesis at high leaf temperature [11] [12]. This effect is reversible for temperature stress exposure below 40°C [13]. However, a too high leaf temperature has irreversible effects on the photosynthesis apparatus, leading to leaf damage and senescence [14]). This direct effect of heat impacts the productivity of plants in the long term by reducing the leaf area index (LAI) so that eventually the plant will need to invest carbon to fix damage and flush new leaves [15]. If the effect of droughts has been widely studied [16], the effect of heat stress, especially on the long term, has not been properly evaluated at regional to global scales for different types of vegetation [17]). This is due to the difficulty in disentangling the direct effect of heat itself from the one of covariates atmospheric dryness and soil moisture deficit. Recently [18] made a first attempt to evaluate the temperature threshold of heat impact on vegetation and the increasing probability of reaching this critical temperature. To go a step further it is important to quantitatively assess the impact of heat stress on vegetation functioning, and evaluate the consequence on plant productivity for the future.

Although heat stress is known to be an important factor of crop yield reduction [19, 20] and is considered in most crop models, [21][22], its impact on other ecosystems, in particular forests, remains largely unknown. In land surface models (LSM), the temperature response of photosynthesis allows simulating the short term inhibition of photosynthesis to high temperatures [11] [23] which arises over 35°C; however the long term effect of high temperature, through impaired photosystems, accelerated leaf senescence and turnover, leading to a legacy reduction of LAI, is not considered. LSMs therefore underestimate the effect of heat stress on productivity of terrestrial ecosystems, [24].

Because of their low albedo, leaves absorb a large fraction of incoming sunlight and leaf temperature tends to increase during the day. When soil water is not limiting, the plant can maintain a transpiration flux that keeps the leaf temperature close to the air temperature, [25]. However, during severe droughts, stomatal closure reduces the transpiration flux, and the sensible heat flux cannot evacuate all the incoming energy, which impairs the ability of the plant to regulate its leaf temperature. Without cooling from transpiration, the leaf temperature can reach several degrees above the air temperature [26], amplifying the heat stress. The expected increase of heatwaves associated with droughts in the future [27] should increase the probability that leaf temperature crosses a temperature which provokes irreversible damage to leaves [28], this effect can be further enhanced by the increasing CO2 in dampening transpiration [29].

Improving our understanding of the effect of heat stress over large scales for the different ecosystems is urgent, so that this effect can be included in land surface models for more reliable predictions of ecosystems resilience under climate change. This study addresses this question by quantifying the decrease in vegetation leaf area index (LAI) induced by the direct effect of heat stress using remote sensing estimates of LAI and vegetation indices and surface temperature. Our approach (see method, 2.2) allows the detection of a critical surface temperature over which LAI is impacted by heat stress. This quantification of a critical temperature from remote sensing data is taken into a new parameterisation of leaf turnover related to heat stress in the ORCHIDEE LSM [30]. With this improved model, we then evaluated the impact of heat stress on vegetation productivity during the historical period and until the end of the century using several climate scenarios.

1.1 Observed extreme temperatures

The maximum daily surface temperature (LST) each year was calculated using two different remote sensing products: from Copernicus using geostationary satellites with a time step of one hour and, the second from MODIS with two points in the day at 10:30 am and 1:30 pm (see data description in section 2.1.1). Figure 1a shows the map of observed maximum daily temperature each year from Copernicus dataset over the period (2011-2019), and Figure 1b gives the year when this maximum temperature is reached. The maximum daily temperature each year varies from 30°C in the high Northern latitudes, to 40°C over tropical forests and reaches up to 60°C over arid and semi-arid vegetation. The year when the maximum dily surface temperature was observed depicts spatially coherent patterns over regions that experienced recent droughts and heatwaves. For instance, we clearly identify the 2015-2016 extreme El Niño period over the Amazon [31], the summer droughts and heatwaves in 2011 and 2013 over the southern United States and Mexico [32], in 2018-2019 over

Western Europe [5] and in 2019 in Australia [33]. The comparison between MODIS-LST and Copernicus-LST (fig S1) shows a good agreement between the two LST products as previously noticed by [34] even if MODIS-LST tends to show higher maximum temperature over arid and semi-arid regions an lower values over vegetated areas.

1.2 Anomalies in LAI and vegetation indices related to extreme temperature

Assuming an expected decrease in LAI in the days following exposure to extreme high temperature, we calculated the average LAI one month before and after the day of maximum surface temperature to determine if the maximum temperature is followed by a decrease (or a reduced increase) in LAI. Yet, causes other than heat stress can provoke such an anomaly in LAI. Especially since surface temperature is highly correlated with drought, a decrease of LAI following the maximum temperature due to hydric stress is also expected in addition to the impact of direct thermal stress [35]. To disentangle these two effects, we first determined, for each pixel and each year (called reference year) an analog "LAI" year, i.e., a year during which the LAI time series was the closest to that of the reference year.Selecting two analog years allows to be sure that the two years experience close climate condition in particular in term of water stress which is a maint driver. If the two years experience a different maximum surface temperature. Then we estimated how LAI differs (one month) before and after the time of the yearly maximum temperature defining an heat stress indicator δHS_{ref} (see method 2.2). $\delta HS_{ref} < 0$ means that LAI was more reduced for the hottest year after maximum temperature than for the analog year. We expect a decrease of δHS_{ref} above the a maximum surface temperature which can be considered as the threshold temperature above which leaf damage from direct heat stress occurs. The analysis was conducted on several biomes (i.e Broadleaf deciduous and evergreen forest, needleaf forest, grassland and crops) to identify differential responses of vegetation. In addition, to test the sensitivity of our results to different remote sensing products, we repeated the analysis using the two aforementioned LST products and different vegetation indices (NDVI and EVI2) (see figures S2 to S4 in supplementary material). Figure 2 shows the average of δHS_{ref} normalized by the peak LAI as a function of the maximum LST Ts_{max} estimated from Copernicus-LST for each biomes. The hashed zones represent the confidence interval at 95%. The different biomes show a very similar pattern: the post maximum reduction of LAI δHS_{ref} is almost constant when the maximum temperature is lower than 42°C but a sharp decrease indicating a direct heat negative impact is observed when maximum temperature reach above a threshold of 42°C to 46°C,above witch systematic loss of LAI is observed. Only evergreen broadleaf forests (EBF) show a different behavior with a less sharp decrease after maximum temperature and a high dispersion in δHS_{ref}. If we determine the threshold temperature inducing heat stress damage as the inflection point of the curve (i.e., the temperature at which the second derivative of

δHS_{ref} over Ts_{max} crosses 0), this threshold is around 44°C. The same analysis conducted with MODIS-LST instead of Copernicus-LST shows the same type of response of δHS_{ref} to Ts_{max} (Figure S4), but with a less pronounced decrease above the temperature threshold. The difference might be related to the fact that MODIS measure surface daytime temperature at two fixed time of the day, which is not necessarily the exact time of maximum hourly temperature whereas the Copernicus-LST from geostationary sattelites acquired each 15 minutes allows a more precise characterization of the temperature threshold. Likewise, Figure S2 and S3 show the equivalent of figure 2 for different vegetation indices estimated from MODIS (NDVI, and EVI2) and VGT-NDVI and give the same type of response of δHS_{ref} to Ts_{max}, even if the threshold temperature can be a little different (between 40°C to 44°C), depending on the product and biome. On average the global temperature heat stress threshold is around 43°C It is difficult to conclude why evergreen broadleaf forests gives a different behavior than others biomesas only a few pixels of this biome (less than 2%) reach surface temperatures over 43°C, hence reducing the statistical significance of δHS_{ref}. Nevertheless, these forests predominantly grow in warm and humid conditions (80% of pixels of EBF are located in equatorial moist forest), and are likely able to maintain a sufficient transpiration rate to limit leaf temperature. Moreover, the important cloud cover over these regions also limits the ability to correctly detect the change in remote sensing products around the maximum temperature.

Like for most ecological processes, we can hypothesize that plants adapt their response to heat stress to the local environment. Experiments indeed demonstrated leaf adaptation to heat stress [36]. Hence, we can expect that plants living in regions with high mean annual temperatures have a heat damage temperature threshold higher than plants living in cooler environments. We examined possible local adaptation of the critical temperature above which the heat stress impact becomes significant as a function of mean annual temperature. We assume that a significant impact is reached when $\delta HS_{ref} < -0.2$. This threshold been empirically defined from observed global response on figure 2. Then, for each pixel where $\delta HS_{ref} < -0.2$, we look at the corresponding Ts_{max} which is then assumed to be the local critical temperature Ts_{crit} at which heat stress occurs. Figure 3 represents the distribution of Ts_{crit} as a function of mean annual air temperature for each pixel(Ta_{mean}); The color represents the density of pixels for a given couple Ta_{mean}/Ts_{crit}. We see an increasing trend of critical temperature with mean annual temperature except for the highest ones (R2=0.52). This supports the hypothesis of plant adaptation to heat exposure [36]. We also test the impact of the heat stress duration on δHS_{ref}. For this purpose, we considered the number of days around the maximum temperature for which the maximum temperature stays above 43°C as exposure duration. Figure 4 shows the mean value of δHS_{ref} over the period when LST remains above 43°C as a function of the exposure duration. The heat stress impact increases with the exposure duration but stabilizes if exposure is longer than 5 to 15 days depending of the biome considered, which probably reflects the fact that for heatwaves of long duration most of the top canopy leaves have been affected. For grassland and crops there is an apparent increase of δHS_{ref} for longer periods of heat exposure. Such long periods over 43°C are only located in semi arid regions. We can hypothesize that the fixed 43°C threshold is too low for such regions with high Ta_{mean} as Figure 3 shows that critical threshold for such high temperature region is more around 46°C to 48°C. We also estimated the temporal evolution of the global surface affected by heat stress (figure 5a). Despite an important interannual variation, we observe a positive trend ($1.27.10^4 km^2.year^{-1}$) of surface affected, which indicates an increase of heat stress impact in the last two decades.

1.3 Simulation of the impact of heat stress on the historical period and for the future

Based on the observed relationship between extreme surface temperatures and the LAI decreases above a maximum temperature threshold (figure 2), we implemented a new parameterization in the ORCHIDEE land surface model to represent the impact of heat stress on leaf turnover for each plant functional type (see section 2.3). Simulated maximum surface temperature was similar to the observed one from Cpernicus-LST over the period 2011-2019 , with a small positive bias of around 1°C for the simulated LST compared to observations, and a standard deviation of the differences of 4°C (Figure S5) We then estimated the impact of heat stress on plant productivity by comparing simulations with the standard odel versin (tag 2.2 rev. 6756) (No Heat Stress, NHS) and the new parameterization (Heat Stress, HS). We first conducted a simulation over the historical period (1901-2020) using the CRUJRA 2.2 climate forcing input data. There is a good agreement between the observed increasing trend of surface areas affected by heat stress over the last two decades ($1.27.10^4 km^2.year^{-1}$) and the simulated one (figure 5b) ($1.78.10^5 km^2.year^{-1}$) which correspond to an increasing surface of 1% per year for observation and 1.2% for our simulation. The total affected surface is different, but it is probably related to the difference in spatial resolution between observation (1km) and model (0.5°).

We then evaluated the impact of heat stress on plant productivity with respect to Net Primary Productivity (NPP) simulated by the model. Figure S6b shows the spatial distribution of the simulated impact of heat stress on NPP for the period (1901 to 2020) on annual productivity (NPPHIST-HS − NPPHIST−NHS in percent of NPPHIST−NHS). There is a good coherence between the regions heat exposure triggered an impact on leaf turnover in the model and the subsequent modeled reduction of NPP and the observed regions where a negative δHS_{ref} was observed (figure S6a). The main discrepancy arises in the Sahelian zone and in India where our model simulates a relatively large impact on NPP which does not correspond to an equivalent negative δHS_{ref} in the observations.

The regions that are the most strongly impacted by heat stress are mainly in arid and semi-arid regions, which already experience high maximum surface temperatures (see figure 1). We also plotted the evolution of the global NPP loss induced by heat (in$PgC.year^{-1}$) as the difference between HS and NHS simulations (Figure 6). Globally, there is a slight increase of NPP loss during the 20th century, but it remains limited to 0.1 $PgC.year^{-1}$ before 2000. On the opposite, after the year 2000 the NPP loss increases become more important and reaches 0.16 $PgC.year^{-1}$ in 2020; coherent with previous work on heay stress-induced leaf browning in Bastos et al (2014).

To evaluate the evolution of heat stress impact for the future, we conducted, a series of simulations with and without heat stress effect considering three climate scenarios (RCP2.6, RCP6.0 and RCP8.5) and four Earth System Models (IPSL-CM5-LR, MIROC, HADGEM-ES, GFDL). The impact is evaluated by comparing the NPP simulated with and without heat stress. It should be also noted that during the period 2006 to 2020, the simulated NPP loss (between 0.01 and 0.016 $PgC.year^{-1}$) is largely underestimated compared to the loss simulated using CRUJRA forcing (0.126 $PgC.year^{-1}$)) because in the climate forcing from ISIMIP2, the climate simulated by each model is corrected for its mean bias during the historical period using climate reanalysis. However, the forcing is not corrected to reproduce the observed frequency of extreme events and, as shown by Zhao et al (2021), climate models underestimate the number of drought and heat stress events during the historical period. Another difference if that the ISIMIP2 climate forcing has a daily time step that probably smooths the diurnal temperature evolution compared to CRUJA which is available at 6 hourly time steps. Figure 7 shows the temporal evolution of global heat stress impact on NPP for the three scenarios and the range from four ESMs. Wz found almost no change in the global heat stress impact for scenario RCP2.6 by the end of the century for the different models. For RCP6.0, even if not negligible, the impact is still limited and relatively similar for the different models. On the contrary, a larger impact was predicted with RCP8.5 after 2060, which is largely dependent on the climate model. The global scale impact of heat stress on global NPP is small (2% decrease in the worst case) but regional impacts can be important, with NPP decreasing by up to 25% for instance in China or western USA by the end of the century (Figure S7). There is agreement on the geographical distribution of heat stress impacts on NPP across the four climate models, including east and central North America, Europe, China and north and south tropical bands in Africa and South America. However, climate models disagree on the magnitude of such impacts, the HADGEM climate model leading to the largest decrease in NPP in several regions, most notably over the Amazon. In contrast to the Amazonian forest, the other equatorial forests in Africa and Indonesia are less impacted by heat stress, whatever the simulation. It should be noticed that there is no apparent link between the amplitude of the simulated impact at the end of the 21st century and the agreement with reanalysis over the recent period, as HADGEM climate model gives the second lowest NPP impact for the period 2006-2020. Even if the simulations forced by GFDL and HADGEM climate models show impacts over the Amazonian forest, the regions impacted are different (with

HADGEM climate model the larger impact is observed in western Amazon whereas it is over the east-central Amazon and Brazilian Shield with GFDL climate model). These results indicate that there is a large uncertainty on possible heat stress impacts over the Amazonian tropical forests, which reflect a large difference in the simulated number of days when temperature reaches the threshold that induces heat damage. Furthermore, as mentioned in section 2.2, there are uncertainties in modeling the impact of heat stress for evergreen tropical forests due to the lack of available optical satellite observations (due to cloud coverage) to reliably assess the heat stress impact over the tropics. On the contrary, there is good agreement between climate models for both the spatial patterns and magnitude of the impact of heat stress over China. Considering the underestimation of heat stress impact on the recent period by climate models, we expect that the simulated heat stress impacts for the end of the 21st century are likely to be underestimated.

1.4 Conclusion

Heat stress is known to inhibit photosynthesis and crop productivity, but this impact has rarely been quantified. For natural vegetation, and especially forests, the impact of heat stress on leaves and consequent effects on plant productivity through leaf shedding are still largely unknown. This impact is difficult to assess at large scales because it requires disentangling the effect of heat stress from hydric stress, both being strongly correlated. In this study, we developed a method to estimate the direct impact of heat stress above a maximum temperature exposure based on space-borne estimates of LAI and land surface temperature. We proposed a new proxy of the heat stress impact given by the response of change in LAI around the maximum surface temperature δHS_{ref}, and found that heat stress impacts on LAI begin to be noticeable when the surface temperature exceeds on average, 43°C for most biomes. We further find regional adaptations of this temperature threshold, depending on the mean annual air temperature: this finding tends to indicate that plants growing in hot environments are more tolerant to heat stress. There is also an impact of the duration of the heatwave: the leaf damage increases with heatwave duration over a period between 5 to 15 days, whereas a longer duration has no more effect.

Based on the observed relationship between surface temperature and LAI decrease for the different biomes, we implemented a new parameterization in the ORCHIDEE LSM (v2.2) to represent an increase of leaf turnover at high surface temperatures. We then estimated the climate change-induced heat stress impact on plant productivity both on the historical period (1901-2020) and for the future (2020-2100) considering three climate scenarios simulated by four climate models. The impact slowly increased until the end of the 20th century, but it almost doubled over the last 20 years, reaching up to 0.16 $PgC.year^{-1}$, in agreement with the recent increasing trend of areas affected by heat stress as observed from satellites. For the future, the climate change-induced impact is low for the RCP 2.6 scenario, still limited for RCP6.0 but becomes large for RCP8.5. This is however largely dependent on the considered climate model. While the global impact is limited (2% for HADGEM under RCP8.5), annual NPP can decrease up to 25% in some regions. Several potential vulnerable regions were identified, namely the Amazon humid forests, China, Western Europe and the USA. For the Amazon forest, large uncertainty remains due to the limited number of observations from optical space-borne sensors to constrain the heat stress parameterization, and the discrepancies between simulated impact for the different climate forcing fields. On the contrary, some regional impacts are very consistent between models, for example over China. Recent observations and historical model simulations indicate a doubling of heat stress impacts over the past two decades. Even if the effect of heat stress is currently limited to relatively hot and dry regions, it can be amplified and extended to more regions by increasing temperature and more frequent droughts. It can thus become a concern for the future, even for temperate regions and possibly for the Amazon rainforest.

2 Method

2.1 Data

2.1.1 Surface temperature

We used two different datasets to estimate the daily maximum surface temperature. The first one is the Copernicus hourly land surface temperature dataset Freitas et al (2013) covering the period from January 2011 up to December 2019 with a spatial resolution of 5km. The second dataset is the MODIS TERRA/AQUA 4 days 1km dataset (MOD21A1D.061, https://doi.org/10.5067/MODIS/MOD21A1D.061). The Copernicus dataset has a not a full spatial coverage at a spatial resolution of (5 km) and a temporal resolution of 1 hour over 8 years). MODIS as a spatial resolution of 500m over 21 years In contrast to the Copernicus which gives hourly temperature, the MODIS instruments enable the acquisition of only a single daytime value around 1:30pm local time. MOD21A1D.061 is aggregated to a 4-day time step to limit the cloud contamination.

2.1.2 Leaf area index and vegetation indices

We used the 500m MODIS 4-day composite LAI product (MCD15A3H.061, https://doi.org/10.5067/MODIS/MCD15A3H.061) averaged to 1km, available from 2003 to 2021 To test the robustness of the approach, we also used three sets of vegetation indices covering the period 2001 to 2019. First we used the 1km normalized difference vegetation index (NDVI) 10-day synthesis from SPOT-VGT and PROBA-V available on the Copernicus portal ([37]) (https://www.copernicus.eu/en/access-data/copernicus-services-catalogue/normalised-difference-vegetation-index-1999-2020-raster-1). Second, we used the MODIS 1km 8-day composite reflectances (MCD12Q1.061, https://doi.org/10.5067/MODIS/MCD12Q1.061) from which we estimated two vegetation indices: NDVI, and Enhanced vegetation index v2 (EVI2) ([38]).

To filter the remote sensing time series, we used the Best Indice Slope Extraction (BISE) method [39]. Although originally designed for NDVI, it can be applied to any remote sensing data for which cloud contamination induces a decrease of the value. We thus used the method to filter the different VI indices, but also the LAI and surface temperature. For each couple of VI or LAI vs surface temperature, the data with the highest resolution were averaged to the spatial resolution of the product with the lowest one. So for instance VIs and LAI were binned at the 5 km resolution of the MSG surface temperature dataset; on the contrary, the 500m MODIS surface temperature data were binned at 1km, consistent with the resolution of the VIs and LAI data. To be able to evaluate the response for the main biomes, a time series per pixel was associated with each biome. To do so, we firstly associated each 1km pixel to a unique biome based on the dominant biome estimated from the original 300m ESA-CCI land cover map. When averaged on the 5km grid, for comparison with Copernicus surface temperature, then a mosaic of vegetation was considered, Then different biomes and their associated LAI or vegetation index was considered.

2.1.3 Vegetation maps

To evaluate the results taking into account for different biomes, we use the high resolution ESA-CCI 300m land cover map [40] for the year 2015, and grouped the initial 23 vegetation types into 6 main biomes (Crop, Grassland, Broadleaf evergreen forest, Broadleaf deciduous forest, Needleleaf evergreen forest). We first considered the dominant biome at 1km, the resolution of LAI and vegetation indices. When using the 5km MSG surface temperature we consider a mosaic of vegetation and there corresponding LAI or vegetation index. For the global scale simulations with ORCHIDEE (0.5°x0.5° resolution), we used the vegetation maps produced for the TRENDY intercomparison project [41] which is based on a combination of ESA-CCI maps with the HYDE database of land use change and converted to the 13 ORCHIDEE PFTs [42]. We also considered year 2015 for the global land cover map, albeit land cover varies from one year to the other, since we aim at only evaluating the impact of heat stress (land use change is therefore neglected).

2.1.4 Air temperature and soil water content

For the estimation of 2m air temperature and soil water content, we used the global ERA5 Land product at hourly / 0.1° resolutions covering the period from 1979 up to now [43] (https://cds.climate.copernicus.eu/cdsapp#!/dataset/reanalysis-era5-land?tab=overview) . The data was downscaled to the 5km resolution of the surface temperature data (see 2.1.1) by a linear interpolation with a correction for altitude. For soil water, we only made a bilinear interpolation.

2.1.5 Climate forcing for historical and future simulations

Two climate datasets have been used to conduct the ORCHIDEE simulations. For the historical period (1901 to 2020), we used the CRUJRA V2.2 reanalysis [44], at a 0.5° spatial resolution and six hourly temporal resolution. For the future scenarios, we used the down-scaled, bias-corrected, climate dataset from ISIMIP2 based on AR5 climate scenarios [45] from four different models - IPSL-CM5, HADGEM, GFDL, MIROC - combined to three different representative concentration pathways (RCPs) - RCP2.6, RCP6.0 and RCP 8.5 - at 0.5°/ daily resolutions.

2.2 Detection of the heat stress impact from remote sensing data

The method is based on the differential behavior of the LAI evolution before and after the time of daily maximum surface temperature using two analog years in terms of LAI evolution before the heat period but with a different maximum surface temperature. Comparing two analog years allowed us to eliminate first order driving factors of LAI variation including drought.

First, for each pixel, and for each year (named reference year), we determined the yearly maximum surface temperature Ts_{max} (°C) and the date $d_{Ts_{max}}$ (DOY) at which this maximum occurs. We only selected pixels with sufficient vegetation cover (defined by a mean annual LAI value above 0.5) and for which Ts_{max} was reached during the vegetative period (mean LAI $>$ 0.5 during one month after $d_{Ts_{max}}$). Let X be the variable that characterizes vegetation development (i.e., LAI or one of the vegetation indices considered). We searched for an analog year (i.e., the year which minimizes the difference between the variable X during the vegetative period. Let ΔX the X difference between year y and year y_{ref}:

$$\Delta X(y) = \sum_t X_{y_{ref}}(t) - X_y(t) \tag{1}$$

We then select the year y_a where $\Delta X_{y_a} = min_y(\Delta X(y))$. The pixel is only considered if $Ts_{max}(y_{ref}) > Ts_{max}(y_a)$. In other words, we determined pixels for which a pair of years gave a similar X pattern during the vegetative period but experienced a different Ts_{max}a. If surface temperatures durably affect the foliage, we expect a differential response of the X before and after $d_{Ts_{max}}$. We considered a period of 30 days before and after $d_{Ts_{max}}$, and note ζ_y the difference in X before and after $d_{Ts_{max}}$:

$$\zeta_y = \sum_{t=d_{Ts_{max}}}^{t=d_{Ts_{max}+30}} X_y(t) - \sum_{t=d_{Ts_{max-30}}}^{t=d_{Ts_{max}}} X_y(t) \tag{2}$$

then δ_{ref}, the anomaly of X related to $d_{Ts_{max}}$ on reference year compare to analog year is defined as:

$$\delta HS_{ref} = \zeta_{y_{ref}} - \zeta_{y_a} \tag{3}$$

If heat stress impacts X in the reference year but not on year y_a, then δHS_{ref} should be negative. One can argue that despite the selection of analog years, if the reference year experience an higher water stress than for analog year, δHS_{ref} could also be negative. In this case, the evolution of LAI and soil water content around the time of maximum temperature should be correlated. Hence calculating δSWC_{ref} equivalent to δHS_{ref} but calculated from soil water content instead of LAI should be correlated with δHS_{ref}. We then calculated the Pearson correlation coefficient between δHS_{ref} and δSWC_{ref} for each vegetation type which is always not significant (less than +0.09). This means that differential change of LAI after a high surface temperature period is not associated to a coincident change in soil water content which exclude that the observed LAI decrease has been caused by decrease of soil water.

2.3 Implementation of a heat stress function in ORCHIDEE

Based on the observed impact of heat stress, we implemented a new function in ORCHIDEE to consider the effect of heat stress on the leaf turnover. Where the surface temperature is greater than a threshold θ (°C), we set a daily leaf heat stress turnover $\tau(gC.day^{-1})$, which depends on the temperature exceeding the heat stress threshold and an impact coefficient $\gamma(gC.gC^{-1}.day^{-1}.K^{-1})$ dependent on the PFT. To reflect the saturating effect of heat stress on leaf turnover we assume an upper limit to τ based on lower observed limit of δHS_{ref} (see table 1) Then τ can be estimated as:

$$\tau = min(\tau_{max}, e^{(Ts-\zeta)/2.}/\gamma) \tag{4}$$

We also assumed a limited duration of LAI turnover after heat stress as observed in Figure 4. We then limited the increased turnover to 10 days even if temperatures stayed above ζ for a longer period. The different parameters (θ, γ,τ_{max}) are calibrated from figure 2 for each ORCHIDEE PFT and summarized in table 1. To evaluate the impact of heatstress on NPP we consider couple of simulations where the heat stress additional leaf turnover is activated (HS) or not (i.e standard ORCHIDEE, NHS)

Acknowledgement. *This work was granted access to the HPC resources of TGCC under the allocation 2021-A0090106328 made by GENCI.*

References

[1] Teskey, R. *et al.* Responses of tree species to heat waves and extreme heat events. *Plant, Cell and Environ.* **38**, 1699–1712 (2014). URL https://doi.org/10.1111/pce.12417.

[2] Rao, M. P. *et al.* Approaching a thermal tipping point in the eurasian boreal forest at its southern margin. *Communications Earth & Environment* **4**, 247 (2023).

[3] Sousa, P. M. *et al.* Distinct influences of large-scale circulation and regional feedbacks in two exceptional 2019 european heatwaves. *Communications Earth & Environment* **1**, 1–13 (2020).

[4] Fischer, E., Sippel, S. & Knutti, R. Increasing probability of record-shattering climate extremes. *Nature Climate Change* **11**, 689–695 (2021).

[5] Vautard, R. *et al.* Human contribution to the record-breaking June and July 2019 heatwaves in Western Europe. *ENVIRONMENTAL RESEARCH LETTERS* **15** (2020).

[6] Philip, S. Y. *et al.* Rapid attribution analysis of the extraordinary heatwave on the pacific coast of the us and canada june 2021. *Earth System Dynamics Discussions* **2021**, 1–34 (2021). URL https://esd.copernicus.org/preprints/esd-2021-90/.

[7] Ciais, P. *et al.* Europe-wide reduction in primary productivity of europe caused caused by the heat and drought in 2003. *Nature* **437**, 529–533 (2005).

[8] Bastos, A., Gouveia, C., Trigo, R. & Running, S. W. Analysing the spatio-temporal impacts of the 2003 and 2010 extreme heatwaves on plant productivity in europe. *Biogeosciences* **11**, 3421–3435 (2014).

[9] Van Der Woude, A. M. *et al.* Temperature extremes of 2022 reduced carbon uptake by forests in europe. *nature communications* **14**, 6218 (2023).

[10] Medrano, H., Escalona, J. M., Bota, J., Gulías, J. & Flexas, J. Regulation of photosynthesis of c3 plants in response to progressive drought: stomatal conductance as a reference parameter. *Annals of botany* **89**, 895–905 (2002).

[11] Berry, J. & Bjorkman, O. Photosynthetic response and adaptation to temperature in higher plants. *Annual Review of plant physiology* **31**, 491–543 (1980).

[12] Salvucci, M. E. & Crafts-Brandner, S. J. Inhibition of photosynthesis by heat stress: the activation state of rubisco as a limiting factor in photosynthesis. *Physiologia plantarum* **120**, 179–186 (2004).

[13] Haldimann, P. & Feller, U. Inhibition of photosynthesis by high temperature in oak (quercus pubescens l.) leaves grown under natural conditions closely correlates with a reversible heat-dependent reduction of the activation state of ribulose-1, 5-bisphosphate carboxylase/oxygenase. *Plant, Cell and Environ.* **27**, 1169–1183 (2004).

[14] Akter, N. & M, R. I. Heat stress effects and management in wheat. a review. *Agronomy for sustainable development* **37**, 1–17 (2017).

[15] Ruehr, N. K., Grote, R., Mayr, S. & Arneth, A. Beyond the extreme: recovery of carbon and water relations in woody plants following heat and drought stress. *Tree physiology* **39**, 1285–1299 (2019).

[16] Lipiec, J., Doussan, C., Nosalewicz, A. & Kondracka, K. Effect of drought

and heat stresses on plant growth and yield: a review. *International Agrophysics* **27**, 463–477 (2013).

[17] Breshears, D. D. *et al.* Underappreciated plant vulnerabilities to heat waves. *New Phytologist* **231**, 32–39 (2021).

[18] Li, X. *et al.* Increased crossing of thermal stress thresholds of vegetation under global warming. *Global Change Biology* **30**, e17406 (2024).

[19] Fahad, S. *et al.* Crop production under drought and heat stress: Plant responses and management options. *Frontiers in Plant Science* **8** (2017). URL https://www.frontiersin.org/article/10.3389/fpls.2017.01147.

[20] Semenov, M. A. & Shewry, P. R. Modelling predicts that heat stress, not drought, will increase vulnerability of wheat in europe. *Scientific Reports* **1**, 66 (2011). URL https://doi.org/10.1038/srep00066.

[21] Rezaei, E. E., Webber, H., Gaiser, T., Naab, J. & Ewert, F. Heat stress in cereals: Mechanisms and modelling. *European Journal of Agronomy* **64**, 98–113 (2015).

[22] Prasad, P., Staggenborg, S. & Ristic, Z. Impacts of drought and/or heat stress on physiological, developmental, growth, and yield processes of crop plants. *Response of crops to limited water: Understanding and modeling water stress effects on plant growth processes* **1**, 301–355 (2008).

[23] Sage, R. F. & Kubien, D. S. The temperature response of c3 and c4 photosynthesis. *Plant, cell & environment* **30**, 1086–1106 (2007).

[24] Schewe, J. *et al.* State-of-the-art global models underestimate impacts from climate extremes. *Nature communications* **10**, 1–14 (2019).

[25] Dong, N., Prentice, I., Harrison, S. P., Song, Q. & Zhang, Y. Biophysical homoeostasis of leaf temperature: A neglected process for vegetation and land-surface modelling. *Global Ecology and Biogeography* **26**, 998–1007 (2017).

[26] Gonzalez-Dugo, V. *et al.* Almond tree canopy temperature reveals intra-crown variability that is water stress-dependent. *Agricultural and Forest Meteorology* **154**, 156–165 (2012).

[27] Zscheischler, J. *et al.* Future climate risk from compound events. *Nature Climate Change* **8**, 469–477 (2018).

[28] Akter, N. & Rafiqul Islam, M. Heat stress effects and management in wheat. a review. *Agronomy for sustainable development* **37**, 1–17 (2017).

[29] Obermeier, W. A. *et al.* Reduced co2 fertilization effect in temperate c3 grasslands under more extreme weather conditions. *Nature Climate Change* **7**, 137–141 (2017).

[30] Krinner, G. *et al.* A dynamic global vegetation model for studies of the coupled atmosphere-biosphere system. *Global Biogeochemical Cycles* **19** (2005).

[31] Jiménez-Muñoz, J. C. *et al.* Record-breaking warming and extreme drought in the amazon rainforest during the course of el niño 2015–2016. *Scientific reports* **6**, 1–7 (2016).

[32] Zhang, L., Jiao, W., Zhang, H., Huang, C. & Tong, Q. Studying drought phenomena in the continental united states in 2011 and 2012 using various

drought indices. *Remote sensing of environment* **190**, 96–106 (2017).

[33] Zhang, Y. *et al.* The 2020 special report of the mja–lancet countdown on health and climate change: lessons learnt from australia's "black summer". *Medical journal of Australia* **213**, 490–492 (2020).

[34] Fu, Z. *et al.* Global critical soil moisture thresholds of plant water stress. *Nature Communications* **15**, 4826 (2024).

[35] Caccamo, G., Chisholm, L., Bradstock, R. A. & Puotinen, M. Assessing the sensitivity of modis to monitor drought in high biomass ecosystems. *Remote Sensing of Environment* **115**, 2626–2639 (2011).

[36] Ahrens, C. W. *et al.* Repeated extreme heatwaves result in higher leaf thermal tolerances and greater safety margins. *New Phytologist* **232**, 1212–1225 (2021).

[37] Smets, B. Normalized difference vegetation index (ndvi) collection 300m version 1., product user manual. Tech. Rep., ESA (2016).

[38] Jiang, Z., Huete, A. R., Didan, K. & Miura, T. Development of a two-band enhanced vegetation index without a blue band. *Remote sensing of Environment* **112**, 3833–3845 (2008).

[39] Viovy, N., Arino, O. & Belward, A. The best index slope extraction (bise): A method for reducing noise in ndvi time-series. *Int. J. Remote Sens.* **13**, 1585–1590 (1992).

[40] Defourny, P. Land cover cci product user guide version 2. Tech. Rep., ESA (2017).

[41] Friedlingstein, P. *et al.* Global carbon budget 2023. *Earth System Science Data* **15**, 5301–5369 (2023).

[42] Krinner, G. *et al.* A dynamic global vegetation model for studies of the coupled atmosphere-biosphere system. *GLOBAL BIOGEOCHEMICAL CYCLES* **19** (2005).

[43] Muñoz-Sabater, J. *et al.* Era5-land: A state-of-the-art global reanalysis dataset for land applications. *Earth System Science Data* **13**, 4349–4383 (2021).

[44] Harris, I. Cru jra v2.2: A forcings dataset of gridded land surface blend of climatic research unit (cru) and japanese reanalysis (jra) data; jan.1901 - dec.2020. *NERC EDS Centre for Environmental Data Analysis* (2021).

[45] Hempel, S., Frieler, K., Warszawski, L., Schewe, J. & Piontek, F. A trend-preserving bias correction : the isi-mip approach. *Earth System Dynamics* **4**, 219–236 (2013). URL https://esd.copernicus.org/articles/4/219/2013/.

PFT	$\tau_{max}(gC.gC^{-1}.day^{-1})$	$\theta(C)$	$\gamma(gC.gC^{-1}.day^{-1}.C^{-1})$
Trop. Broad. Ever.	0.04	47	400
Trop. Broad Dec.	0.04	45	650
Temp. Needle. Ever.	0.04	43	700
Temp. Broad. Ever.	0.04	46	550
Temp. Broad. Dec.	0.04	40	600
Bor. Needle. Ever.	0.04	40	700
Bor. Broad. Dec.	0.04	40	600
Bor. Needle. Dec.	0.04	40	800
C3 grassland	0.04	43	600
C4 grassland	0.04	48	600
C3 crop	0.04	43	600
C4 crop	0.04	48	600

Table 1 parameters of the 12 PFTS for heat stress parameterisation in ORCHIDEE τmax: maximum turnover rate, θ: threshold surface temperature triggering leaf turnover, γ: impact coefficient

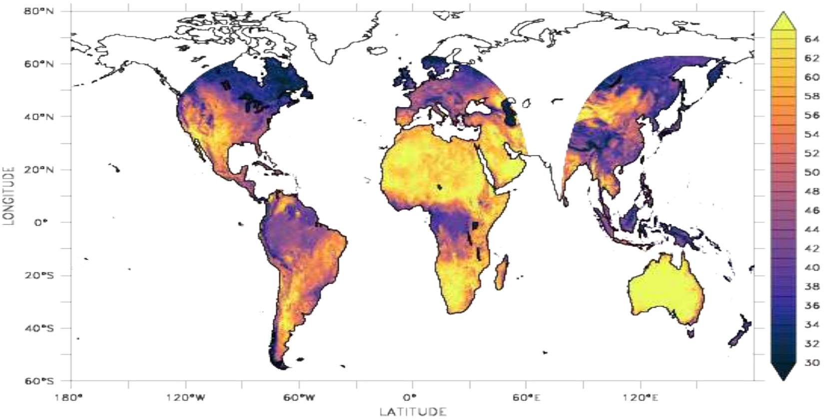

a/

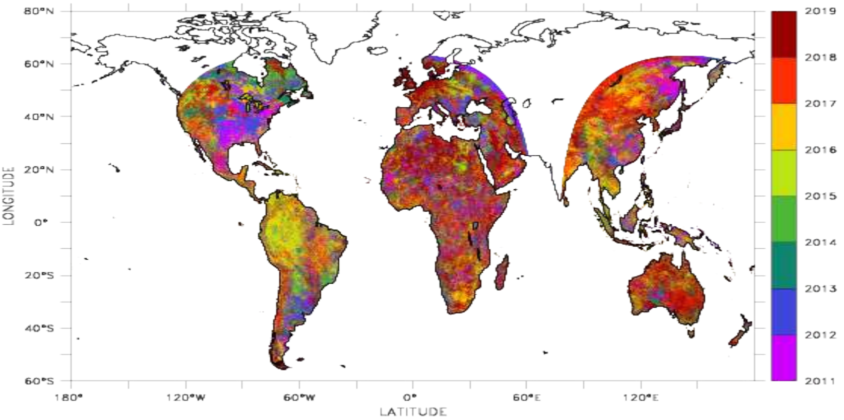

b/

Figure 1 a/maximum surface temperature over 2011-2019 b/ year of the maximum temperature

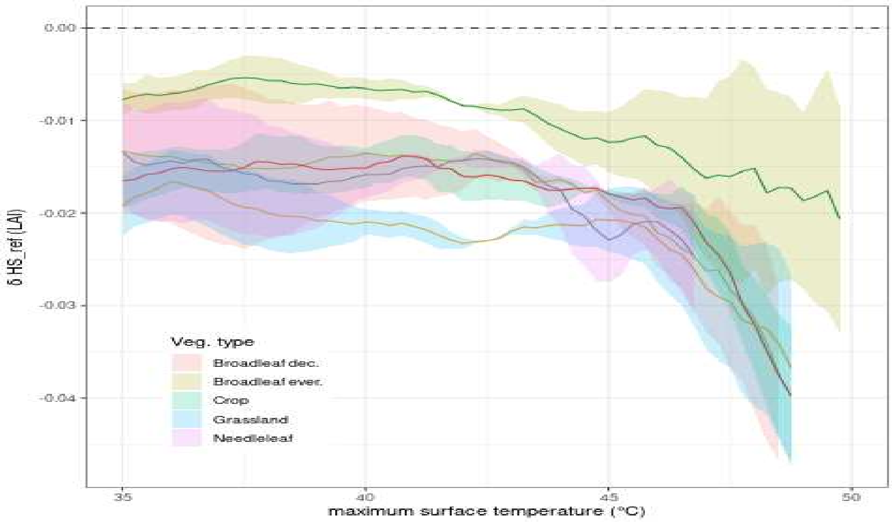

Figure 2 Heat stress indicator δHS_{ref} estimated from MODIS LAI data as a function of Ts_{max} (based on MSG Ts) for the 6 main biomes and confidence interval at 95%

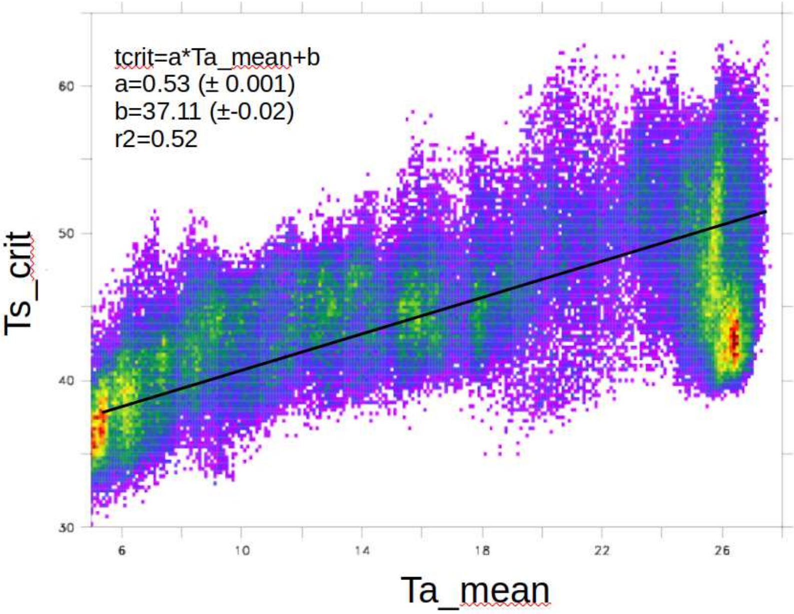

Figure 3 threshold Ts_{max} versus mean annual temperature (Ta_{mean}) when δHS_{ref}<-0.2

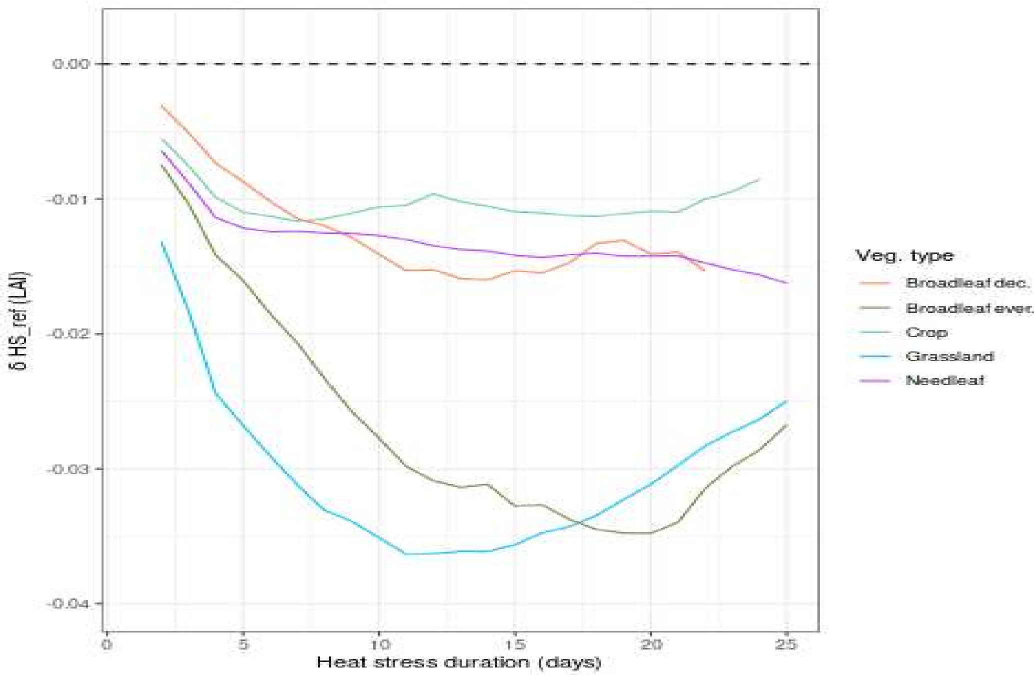

Figure 4 Observed δHS_{ref} (based on MODIS LAI) as a function of heat stress duration (number of days over 43°C)

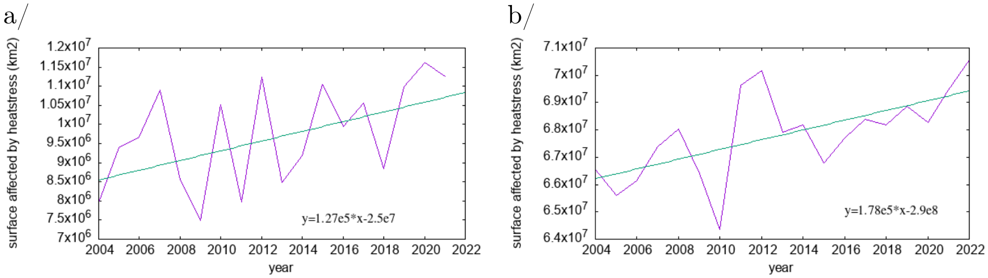

Figure 5 a/ mean δHS_{ref} b/ yearly variation of the surface areas affected by heat stress. Based on MODIS-LAI and MODIS-LST for the period 2004-2021

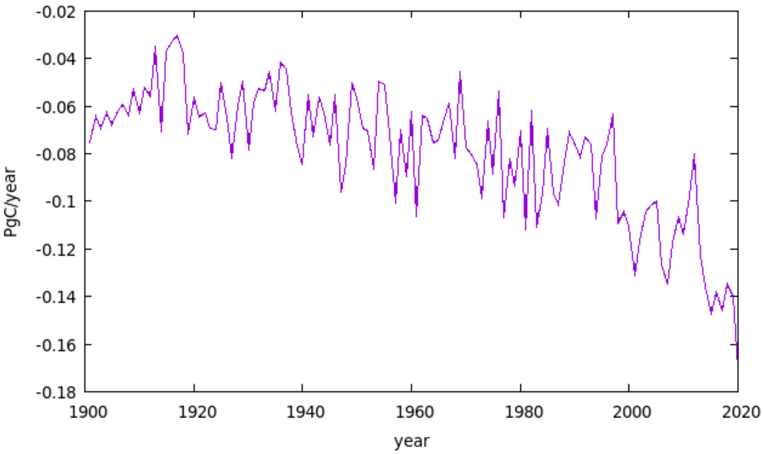

Figure 6 Simulated evolution of global loss of NPP ($PgC.year^{-1}$) induced by heat stress from 1901 to 2020

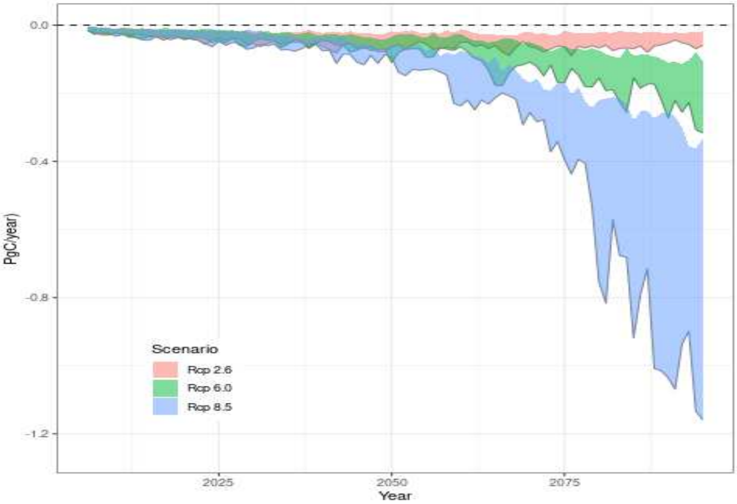

Figure 7 Evolution of the heat stress global impact on NPP for the 3 RCPs scenarios. Hatched zones represent the min and max of the 3 models

Supplementary information.

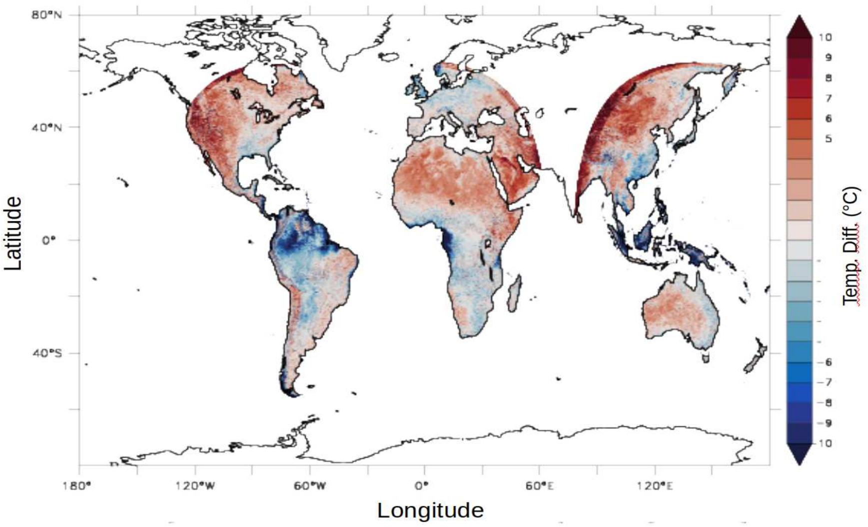

Figure S1 Difference in mean of maximum yearly temperature (K) between MODIS and MSG over the period 2011-2019

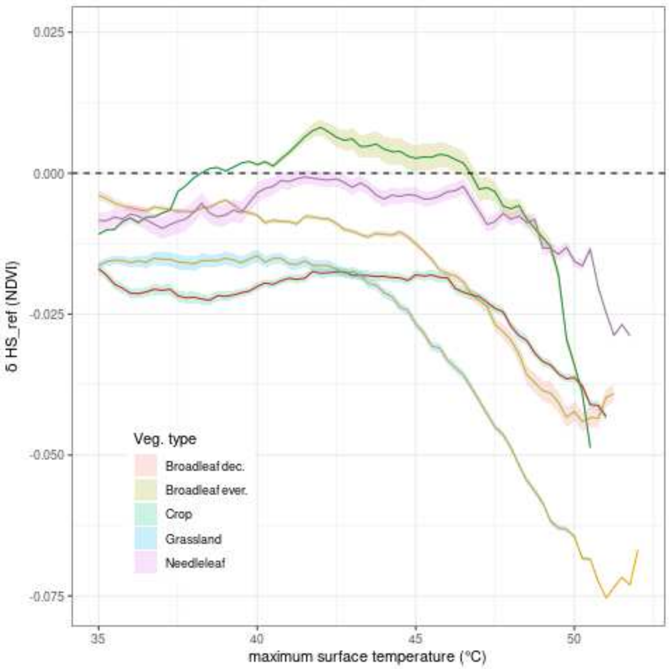

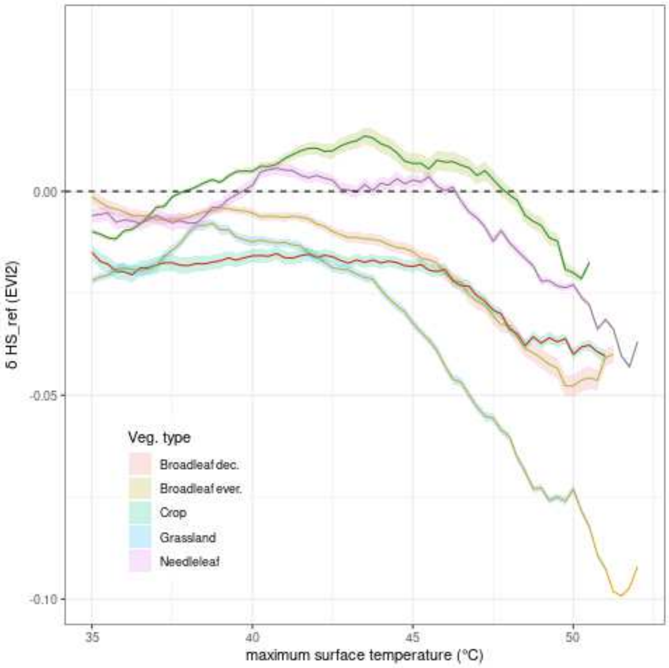

Figure S2 Observed δHS_{ref} (based respectively on MODIS NDVI and MODIS EVI2) as a function of Ts_{max} (based on MODIS-Ts) for the 6 main biomes and confidence interval at 95%

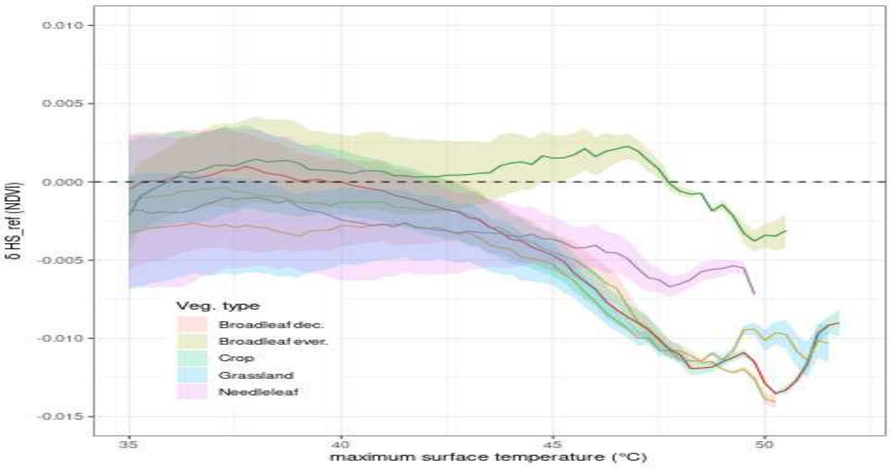

Figure S3 Observed δHS_{ref} based on VGT NDVI as a function of Ts_{max} (MSG Ts) for the 6 main biomes and confidence interval at 95%

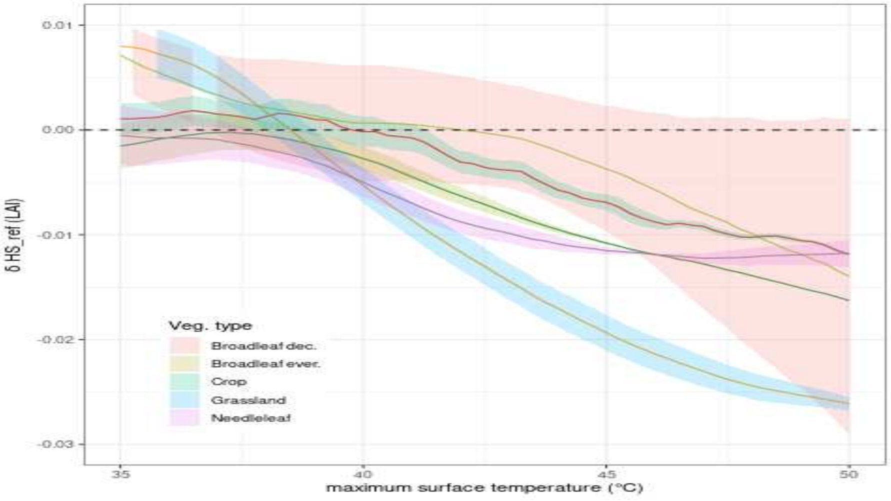

Figure S4 Observed δHS_{ref} based on MODIS LAI as a function of Ts_{max} (MODIS Ts) for the 6 main biomes and confidence interval at 95%

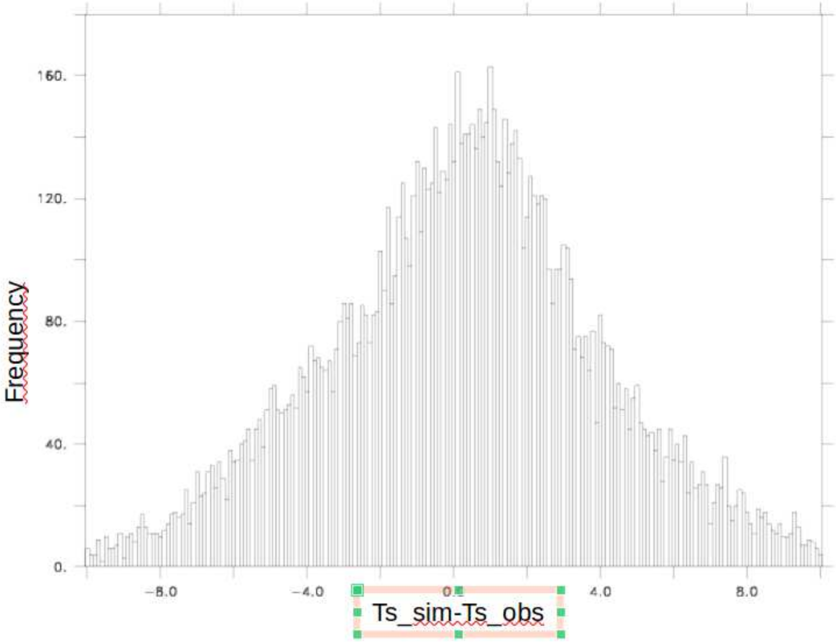

Figure S5 Histogram of differences between simulated and observed maximum surface temperature for 2011 to 2021

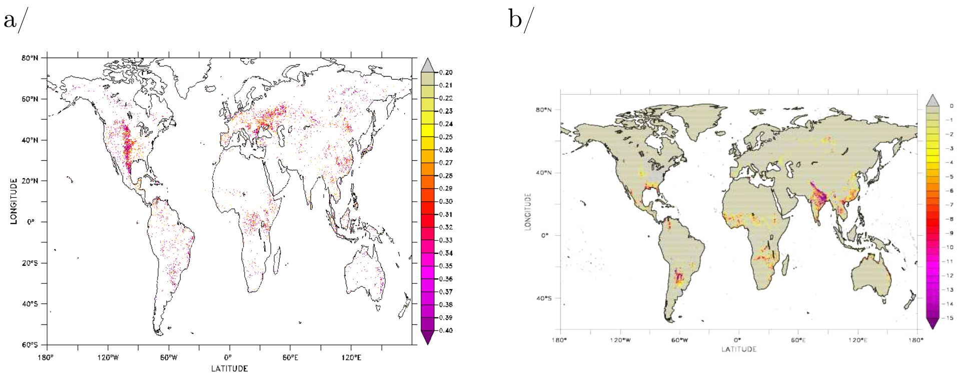

Figure S6 a/ mean of δHS_{ref} for $\delta HS_{ref} < 0$ indicating regions affected by heat stress b/ Spatial distribution of simulated global mean loss of NPP (%) induced by heat stress leaf turnover from 2004 to 2022

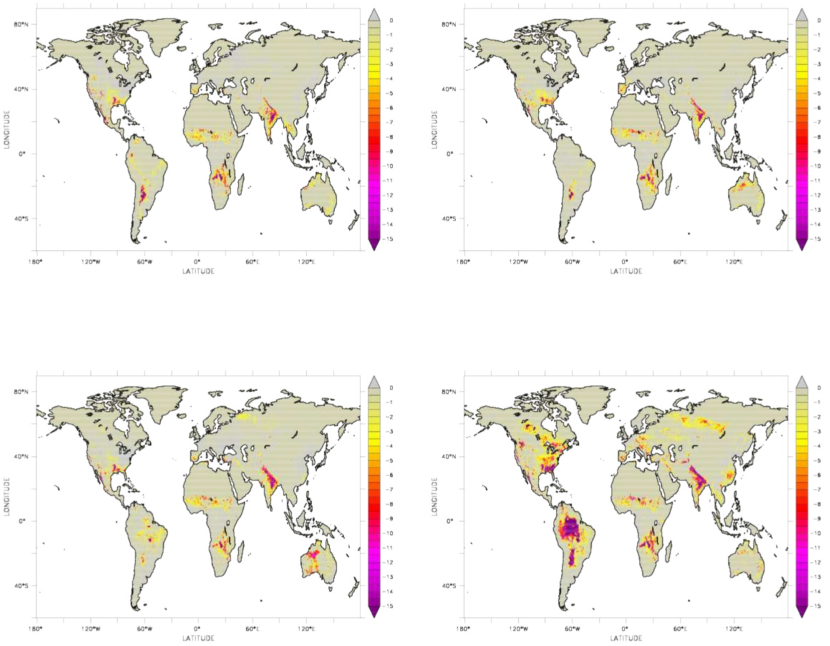

Figure S7 Mean impact of heat stress for the period 2081-2099 on NPP (%) for scenario RCP 8.5, (a) IPSL (b) GFDL (c) MIROC (d) HADGEM